PNAS RESEARCH ARTICLE | IMMUNOLOGY AND INFLAMMATION OPEN ACCESS

Intestinal tissue-resident T cell activation depends on metabolite availability

Špela Konjar[a,1,2], Cristina Ferreira[a], Filipa Sofia Carvalho[a], Patrícia Figueiredo-Campos[a], Júlia Fanczal[a], Sofia Ribeiro[a], Vanessa Alexandra Morais[a], and Marc Veldhoen[a,1]

Edited by Lora Hooper, University of Texas Southwestern Medical Center, Dallas, TX; received February 7, 2022; accepted July 21, 2022

The metabolic capacity of many cells is tightly regulated and can adapt to changes in metabolic resources according to environmental changes. Tissue-resident memory (T_{RM}) $CD8^+$ T cells are one of the most abundant T cell populations and offer rapid protection against invading pathogens, especially at the epithelia. T_{RM} cells metabolically adapt to their tissue niche, such as the intestinal epithelial barrier. In the small intestine, the types of T_{RM} cells are intraepithelial lymphocytes (IELs), which contain high levels of cytotoxic molecules and express activation markers, suggesting a heightened state of activation. We hypothesize that the tissue environment may determine IEL activity. We show that IEL activation, in line with its semiactive status, is metabolically faster than circulating $CD8^+$ T cells. IEL glycolysis and oxidative phosphorylation (OXPHOS) are interdependently regulated and are dependent on rapid access to metabolites from the environment. IELs are restrained by local availability of metabolites, but, especially, glucose levels determine their activity. Importantly, this enables functional control of intestinal T_{RM} cells by metabolic means within the fragile environment of the intestinal epithelial barrier.

IELs | T cells | metabolism | tissue-resident memory T cells | glucose

Significance

The role of tissue-resident memory T cells has come to the forefront, and intestinal intraepithelial lymphocytes (IELs) are abundant. The cells protect the host against invasion and regulate tissue homeostasis and tolerance. Microbial invasion and aberrant IEL activation can contribute to disorders such as inflammatory bowel disease. IELs are kept in a state with limited metabolic activity. We describe the functional analysis of IELs compared with their CD8 circulating counterparts. Although proliferative bursts are similar, IEL metabolism is rapid. Metabolic pathway analysis highlights a tight connection of OXPHOS and glycolysis in IELs and a reliance on pyruvate oxidation. Glucose availability in the local environment can regulate IEL activity, resulting in rapid clearance of an intestinal parasite infection.

The metabolic capacity of many cells is flexible and can be adjusted to changes in metabolic availability according to local changes, such as dietary intake in the intestine. In turn, metabolic programs are associated with specialized cell functions that can change upon availability of required metabolites. Metabolic disorders are increasing in prevalence throughout the world and impacting human physiology, including immune function. The incidence of intestinal bowel disorders has steadily risen over recent decades with largely unknown etiology, although dietary and microbial alterations have been suggested (1). Pathogenic and commensal microorganisms as well as food particles frequently challenge the integrity of the intestinal epithelial barrier.

Intestinal intraepithelial lymphocytes (IELs) are one of the most abundant, intestine-specific, populations of tissue-resident memory T cells (T_{RM}) that provide an important line of immune defense against challenges at the intestinal barrier. The most abundant IEL population expresses the coreceptor CD8 and can be divided into two major subsets. Induced IELs are derived from conventional $CD8\alpha\beta^+TCR\alpha\beta^+$ T cells, the classic T_{RM} cells found in many organs, while $TCR\gamma\delta^+CD8\alpha\alpha^+$ and $TCR\alpha\beta^+CD8\alpha\alpha^+$ T cells represent natural IELs specific to the small intestine (2). IELs have a key role in tissue protection and homeostasis by eliminating infected cells and promoting the production of antimicrobial and epithelial growth factors (3). Activation of IELs can limit acute infection and provoke an innate response from the villus epithelium (4–6). However, their cytotoxic potential and activation readiness requires tight control to avoid aberrant immunity and pathology of the single epithelial layer, with aberrant activity contributing to colitis in mice and humans (7, 8).

Upon activation, quiescent T cells undergo proliferation and acquire effector functions requiring additional metabolic capacity (9–11). Upon recognizing cognate antigen, naïve T cells are retained in the lymph nodes where optimal metabolic conditions are met, prior to migration to the tissues. Upon pathogen clearance, effector T cells die off, while a population of memory T cells is established, involving the deactivation of effector programs. Some memory T cells may take up long-term residence in the previously inflamed tissues, as T_{RM} such as induced IELs. In contrast to circulating memory T cells, at epithelial barriers, the mouse skin, and the small intestine, T_{RM} cells show signs of a heightened state of activation. They contain cytotoxic molecules and express activation markers (2, 6). In the small intestine, an organ specialized in metabolite uptake, the IEL ecosystem comprises specialized cell types, growth factors, altered oxygen pressure, and metabolite availability. This suggests that T_{RM} cells have to undergo metabolic adaption for their survival and functionality (12). Previous studies suggest

Author affiliations: [a]Instituto de Medicina Molecular João Lobo Antunes, Faculdade de Medicina, Universidade de Lisboa, Lisboa 1649-028, Portugal

Author contributions: Š.K., C.F., F.S.C., V.A.M., and M.V. designed research; Š.K., C.F., F.S.C., P.F.-C., J.F., S.R., and M.V. performed research; Š.K., C.F., V.A.M., and M.V. analyzed data; and Š.K., V.A.M., and M.V. wrote the paper.

The authors declare no competing interest.

This article is a PNAS Direct Submission.

[1]To whom correspondence may be addressed. Email: spelakonjar@medri.uniri.hr or marc.veldhoen@medicina.ulisboa.pt.

[2]Present address: Center for Proteomics, Faculty of Medicine, University of Rijeka, 51000 Rijeka, Croatia.

This article contains supporting information online at http://www.pnas.org/lookup/suppl/doi:10.1073/pnas.2202144119/-/DCSupplemental.

Published August 15, 2022.

that IELs have an altered metabolism (5, 6, 13). We hypothesize that the intestinal metabolic environment, altered IEL metabolic wiring, and control of IEL activity are interconnected.

Under steady-state conditions, IELs have not been shown to have additional oxidative phosphorylation (OXPHOS) capacity, readily detected in circulating T cells, to support cellular activity (5, 6, 13). Interleukin (IL)-15, the expression of which is elevated during tissue stress or infection (3), has been reported to increase the mitochondrial respiratory capacity of IELs (14). Skin $CD8^+$ T_{RM} cells, which share characteristics with small-intestinal IELs, also increase expression of metabolic proteins and can utilize mitochondria fatty acid β-oxidation (FAO) to support their long-term survival and function (13). Furthermore, we show that intestinal IELs have an altered mitochondrial makeup of cardiolipins, where the composition of cardiolipin entities correlates with the activation status of IELs (6). An important outstanding question is how IEL activity is regulated. IELs are poised yet impeded for activation, but can swiftly reduce the invading pathogen burden. How this is controlled to prevent aberrant activation and immunopathology remains unknown.

Here we evaluate metabolic changes and requirements of IELs upon in vivo activation. We show that proliferative kinetics between T cell subsets are similar, with metabolic activity near basal levels at the peak of proliferation. Intestinal IEL activation, with increase in OXPHOS, is more rapid compared with circulating $CD8^+$ T cells. However, IEL metabolism is more dependent on direct access to metabolites, especially glucose, and shows a tight interdependency between OXPHOS and glycolysis. Increased glucose availability enhances the IEL antipathogen activity.

Results

T Cell Proliferative Burst Kinetics Are Similar. Proliferation is a key characteristic following T cell activation. To compare the proliferative burst of circulating $CD8^+$ T cells and $CD8^+$ IELs, we used anti-CD3ε antibodies for synchronized in vivo activation (4, 6). Despite its semiactivated status, the IEL proliferative burst peaks at a similar time to circulating $CD8^+$ T cells, 48 h after TCR ligation, with natural CD8αα IELs showing a slightly reduced amplitude compared with induced CD8αβ IELs (Fig. 1 *A*–*D*).

Others and we previously reported limited OXPHOS capacity in IELs (5, 6, 13), readily observed in circulating $CD8^+$ T cells (15). At the peak of proliferation of all $CD8^+$ T cells tested, 48 h post in vivo activation, we analyzed extracellular flux capacity. The oxidative consumption rate (OCR) at this time point is similar to steady state (Fig. 1*E*), with a modest increased basal OCR observed in circulating T cells after activation (Fig. 1*F*). Steady-state basal OCR levels are similar in circulating T cells and IELs, with maximum basal OCR levels raised at the peak of proliferation in circulating T cells (Fig. 1 *F* and *G*). Circulating $CD8^+$ T cells exhibit spare respiratory capacity (SRC), not observed in IELs (Fig. 1 *E* and *H*).

Extracellular acidification rate (ECAR), a readout of pericellular pH that reflects the production of lactate and bicarbonate that can be correlated to glycolysis, is raised in circulating effector T cells 48 h after activation (Fig. 1*I*). At this time, circulating T cells exhibit higher basal and maximum glycolysis rates compared with nonstimulated circulating T cells (Fig. 1 *J* and *K*). The IEL glycolysis rate 48 h after stimulation is similar to basal

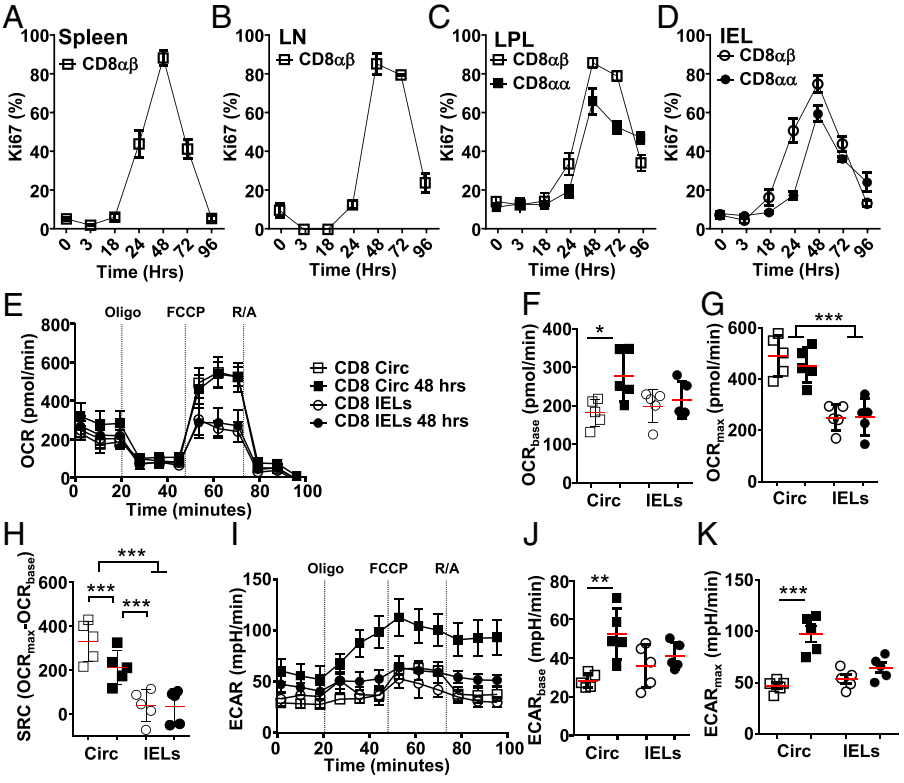

Fig. 1. Proliferation kinetics are similar between circulating and tissue-resident CD8 T cells. C57BL/6J mice were injected i.p. with anti-CD3ε, and, at indicated tissues and time points, $CD8^+$ T cells were assessed. (*A*–*D*) Flow cytometry staining for Ki67 for CD8αβ T cells in spleen (*A*), lymph nodes (LN) (*B*), and CD8αβ and CD8αα T cells in lamina propria (LPL) (*C*), and small-intestinal intraepithelial (IEL) compartment (*D*) (n = 3 to 15 from three biological repeats). (*E* and *I*) Representative extracellular flux analysis (mitostress assay, compounds used at indicated time) for circulating $CD8^+$ T cells from spleen (squares) or small-intestinal IELs (circles) at steady state (open symbols) or 48 h after anti-CD3ε (closed symbols) showing OCR (*E*) and ECAR (*I*). (*F*–*H*, *J*, and *K*) Direct comparisons of basal OCR (*F*), maximum OCR (*G*), SRC (*H*), basal ECAR (*J*), and max ECAR (*K*) all for the samples measured in *E* and *I* (n = 5 to 15, from three biological repeats). Statistical analysis using Mann–Whitney U test; $^*P < 0.05$; $^{**}P < 0.01$; $^{***}P < 0.001$.

rates (Fig. 1 *J* and *K*). Treatment with oligomycin, inhibiting OXPHOS, only engages glycolysis in activated circulating CD8$^+$ T cells. Our data suggest that, at the peak of IEL and circulating CD8$^+$ T cell proliferative burst, OXPHOS and glycolysis levels are already reduced to steady-state levels.

T Cell Metabolic Activity Precedes Proliferation. As present in effector T cells, IELs contain secretory vesicles enclosing cytotoxic proteins such as granzymes (6, 16, 17). In vivo activation of IELs, in line with their proposed rapid response and in marked contrast to circulating T cells, naïve or memory, swiftly increases granzyme B protein content (Fig. 2*A*). The difference in granzyme expression between circulating CD8$^+$ T cells and IELs is not due to changes within each population, such as memory and naïve CD8$^+$ T cells (*SI Appendix*, Fig. S1). This also indicates that IELs were activated and viable at the time of analysis.

Circulating CD8$^+$ T cells may increase their OXPHOS output prior to proliferation as reported in memory T cells (18). Metabolic flux analysis at 16 and 24 h after in vivo activation of circulating CD8$^+$ T cells reveals the highest glycolytic activity in comparison to other time points of in vivo activation (Fig. 2*B*). Additional earlier time points after activation reveal a gradual increase in glycolysis compared with baseline without activation (Ctrl), reaching maximum levels between 16 and 24 h postactivation, with a return to near-steady-state levels by 48 h postactivation (Fig. 2*C*). In circulating CD8$^+$ T cells, OXPHOS shows a more distinct burst of activity at 24 h after activation, reduced to steady-state levels by 48 h after activation (Fig. 2 *D* and *E*). At 24 h after activation, the maximum level of OXPHOS is reached using all SRC available during rest, which is available again 48 h after activation (Figs. 1*E* and 2*D*). Of interest, in circulating CD8$^+$ T cells at 16 h after in vivo activation, basal OXPHOS levels increase without the availability of additional capacity revealed after carbonilcyanide p-triflouromethoxyphenylhydrazone (FCCP) addition (Fig. 2*F*), similar to observations in IELs at rest, 24 or 48 h after activation (Figs. 1*E* and 2*G*) (6).

Our data show that, upon in vivo activation of circulating CD8$^+$ T cells, glycolytic activity gradually increases, peaking at

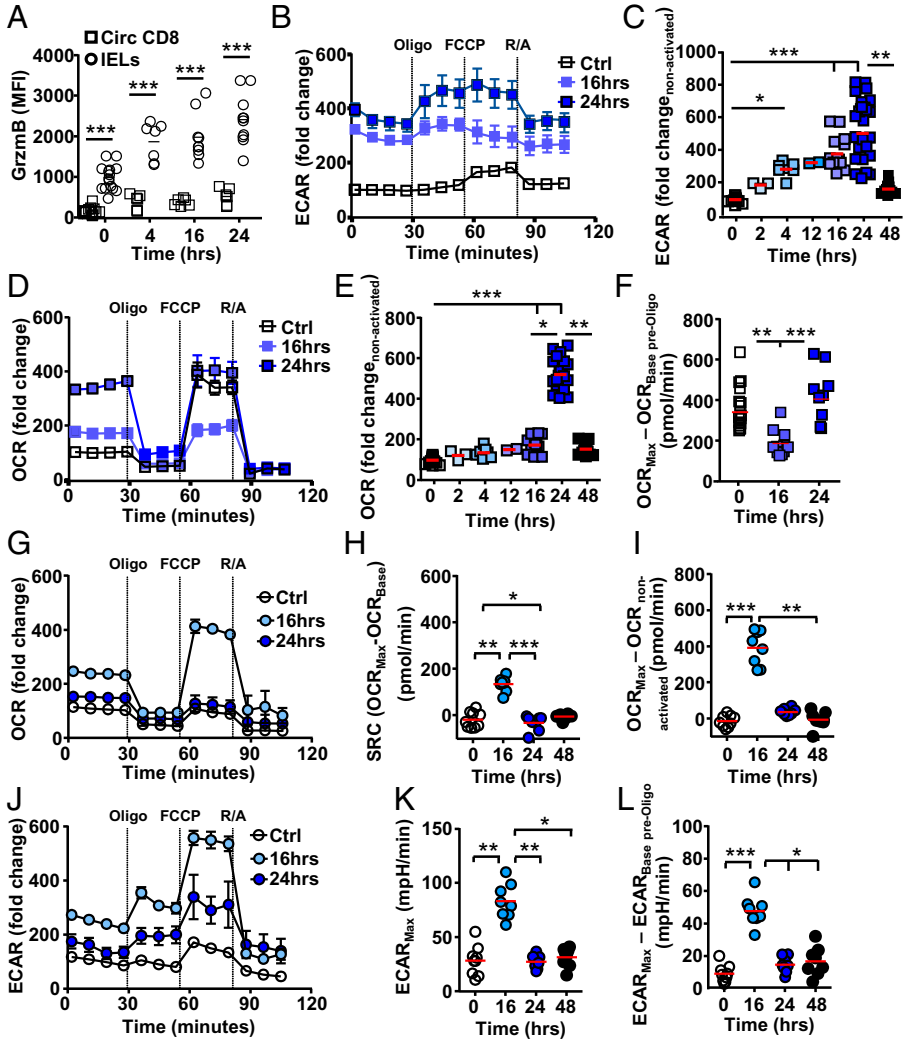

Fig. 2. T cell metabolic activity precedes proliferation. C57BL/6J mice were injected i.p. with anti-CD3ε and at indicated time points, and CD8$^+$ T cells were assessed. (*A*) Flow cytometry intracellular staining for granzyme B (GrzmB) (n = 4 or 5, from three biological repeats) in circulating CD8$^+$ T cells (squares) and IELs (circles). (*B*–*L*) Representative extracellular flux analysis (mitostress assay, with compounds used indicated at time used) from circulating CD8$^+$ T cells assessing (*B* and *C*) ECAR and (*D*–*F*) OCR. Representative extracellular flux analysis of CD8$^+$ IELs assessed for (*G*–*I*) OCR or (*J*–*L*) ECAR. (*C* and *E*) Basal levels normalized to steady-state, nonactivated, ECAR or OCR for circulating CD8 T cells prior to oligomycin addition. (*F*) Comparing maximum OCR level, after FCCP addition, of each condition with OCR levels prior to oligomycin addition in nonstimulated cells. (*I*) OCR levels normalized to nonactivated cells prior to oligomycin addition, (*K*) maximum levels (mpH per minute) upon FCCP injection, and (*L*) ECAR normalized to levels prior to oligomycin addition, within each condition (n = 2 or 3 from two or three biological repeats). Statistical analysis using Mann–Whitney U test; *P < 0.05; **P < 0.01; ***P < 0.001.

24 h or shortly after, at which time a distinct OXPHOS burst takes place. Although circulating CD8$^+$ T cells show OCR capacity at rest, this is blunted early during activation, similar to observations in IELs, prior to being used.

IEL Metabolic Activity Shows a Rapid Burst. IELs show limited OXPHOS activity 24 h after in vivo activation, similar to their resting state (Fig. 2*G*) (5, 6, 13). However, IELs are able to increase OXPHOS soon after activation (Fig. 2 *G–I*) (19). The SRC observed at 16 h after activation, with increased OCR compared with steady state, indicates maximum OXPHOS is reached prior to this time point. Maximum OCR levels reached in IELs are in line with those observed in circulating CD8$^+$ T cells (Fig. 2*G*).

At 16 h post in vivo activation, basal levels of glycolysis increase in IELs (Fig. 2*J*), peaking early, at 16 h or prior, and return to steady-state levels within 24 h (Fig. 2*K*). In contrast to circulating T cells, mitochondrial uncoupling using protonophore FCCP results in increased glycolytic activity in activated IELs especially 16 h after activation (Fig. 2 *B*, *J*, and *L*).

Our data show that circulating CD8$^+$ T cell and IEL activation results in metabolic activity that precedes the proliferative burst. In circulating T cells, glycolytic activity gradually reaches maximum capacity. Their OXPHOS capacity is initially curbed, followed by maximum use and a return to rest with available SRC. IELs at rest are in a metabolic state in which OXPHOS capacity is curtailed. However, they can rapidly increase metabolic activity upon activation and are able to liberate additional OXPHOS capacity. IEL glycolysis appears limited and shows a possible interdependence on OXPHOS, indicating disparate metabolic phenotypes between circulating CD8$^+$ T cells and IELs.

Activated IELs Have Pyruvate Capacity. To identify the metabolic requirements for circulating CD8$^+$ T cells and IELs, we assessed the messenger RNA (mRNA) profile of two previously activated cell populations, circulating memory T cells and IELs (6). No alterations in mRNA levels of enzymes involved in glycolysis or OXPHOS were observed (*SI Appendix*, Fig. S2*A*). We confirmed the expression of the glucose receptors, GLUT1 and GLUT3 (*Slc2a1*, *Slc2a3*). Furthermore, we found differential expression of the sodium/glucose cotransporter (SGLT)1 (*Slc5a1*) on IELs, an adenosine 5′-triphosphate (ATP)-independent sodium-dependent glucose transporter (*SI Appendix*, Fig. S2*B*). Uptake of glucose in T cells is difficult to assess. It depends on the glucose transporters expressed with different uptake kinetics of dyes, often much slower, 50- to 100-fold, compared to glucose (20, 21). The 2-NBDG (2-(N-(7-nitrobenz-2-oxa-1,3-diazol-4-yl)amino)-2-deoxyglucose), a fluorescent glucose analog commonly used, indicated that, at steady state, circulating CD8$^+$ T cells and IELs can take up glucose (Fig. 3*A*). TCR ligation resulted in rapid 2-NBDG visibility in circulating T cells, peaking around 16 h, but no increase in fluorescence was detected in activated and nonactivated IELs (Fig. 3*B*). Modification at the C2 position of glucose, as in 2-NBDG, allows phosphorylation and subsequent degradation during which the fluorescent signal can be lost. Using the nondegradable fluorescent glucose analog 6-NDBG, which, in contrast to 2-NBDG, does not rely on GLUT2 expression, we observed glucose uptake in circulating

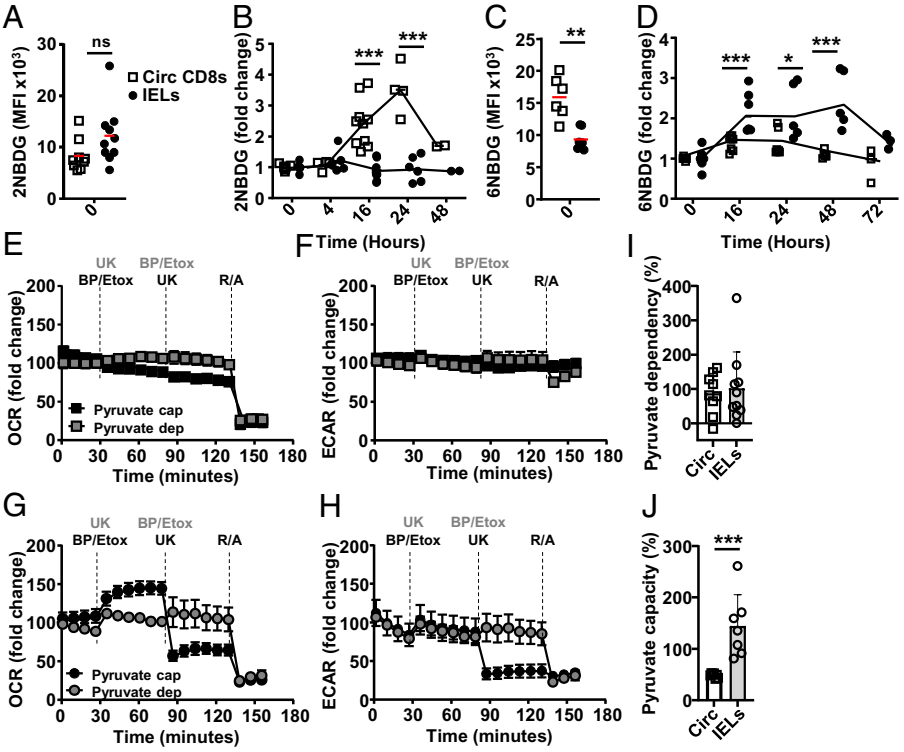

Fig. 3. IELs make use of glycolysis that is coupled to OXPHOS. C57BL/6J mice were injected i.p. with anti-CD3ε, and, at indicated time points, circulating CD8 T cells (squares) and IELs (circles) were assessed for glucose uptake (mean fluorescent intensity [MFI]) at rest (*A* and *C*) or after activation normalized to at rest signal (*B* and *D*) in vitro using 2-NBDG (*A* and *B*) or 6-NBDG (*C* and *D*) (n = 5 or 6, three independent experiments). (*E–J*) Extracellular flux mitofuel assay (compounds used at indicated times) was used to evaluate the dependency or capacity of T cells 16 h after in vivo activation on pyruvate oxidation. Normalized (*E* and *G*) OCR and (*F* and *H*) ECAR levels for (*B* and *C*) circulating CD8$^+$ T cells or (*D* and *E*) IELs upon addition of UK-5099 (UK, pyruvate carrier [MPC] inhibitor) to determine pyruvate dependency (gray symbols, compounds added in gray) or capacity (black symbols and text) after initial inhibition of FAO availability with Etomoxir (Etox) and glutamate availability with BPTES (BP). Addition of R/A served as a control of OXPHOS inhibition and viability. (*I*) Pyruvate dependency of circulating CD8$^+$ T cells and IELs ((baseline OCR – UK-5099 OCR)/(baseline OCR – all inhibitors OCR) × 100%), and (*J*) pyruvate capacity of both T cell subsets (1 − (baseline OCR – PBTES + Etox OCR)/(baseline OCR – all inhibitors OCR) × 100%). Representative of three biological repeats, n = 2 to 4. Statistical analysis using Mann–Whitney *U* test; ns: not significant, $^*P < 0.05$; $^{**}P < 0.01$ $^{***}P < 0.001$.

$CD8^+$ T cells, as seen with 2-NBDG, and revealed 6-NBDG uptake in IELs upon stimulation (Fig. 3 *C* and *D*) (22). Collectively, the data suggest that IELs have glucose capacity and rapidly process the glucose obtained compared with circulating $CD8^+$ T cells.

Glycolysis results in the generation of lactate or pyruvate, the latter used to supply the Krebs cycle and electron transport chain in the mitochondria for optimal ATP production. Pyruvate is not the sole metabolite used in OXPHOS; the main others are lipids and glutamate. We assessed mitochondrial metabolite requirements 16 h after in vivo activation, with high OXPHOS and glycolysis, by targeting either one major metabolic pathway, to assess dependency, while the other two remain available, or by inhibiting two major metabolic pathways simultaneously and the remaining third thereafter, to assess capacity. In line with short-term alterations in glucose availability not affecting OXPHOS, the OCR of circulating $CD8^+$ T cells is independent of glucose when the mitochondrial pyruvate carrier inhibitor, UK-5099, prevents pyruvate reaching the mitochondria (Fig. 3*E*). When the carnitine palmitoyltransferase-1 inhibitor etomoxir and the glutaminase GLS1 inhibitor bis-2-(5-phenylacetamido-1,2,4-thiadiazol-2-yl)ethyl sulfide (BPTES) prevent access to fatty acid (FA) and glutamate, respectively, OXPHOS activity shows no reliance on glucose capacity in circulating $CD8^+$ T cells. At 16 h after in vivo activation, enabling metabolite acquisition (23), OCR and ECAR in circulating $CD8^+$ T cells do not depend on pyruvate, lipid, or glutamate availability within the time of the assay (Fig. 3 *E* and *F*).

OXPHOS levels in IELs, similarly to circulating $CD8^+$ T cells, do not show acute pyruvate dependency; UK-5099 prevents pyruvate shuttling and oxidation in the mitochondria but does not alter OXPHOS activity. However, there is marked capacity for pyruvate oxidation, with OXPHOS relying on it when FA and glutamate are absent (Fig. 3 *G* and *H*). Combined inhibition of FA and glutamine oxidation increases OXPHOS activity, suggesting increased reliance on pyruvate. The determined pyruvate dependency is similar between circulating $CD8^+$ T cells and IELs, while IELs show a markedly higher capacity for pyruvate (Fig. 3 *I* and *J*), indicating that activated IELs present a strong preference for glucose as an energy source. Surprisingly, and in marked contrast to circulating $CD8^+$ T cells, IEL OXPHOS inhibition is mirrored by reduced glycolysis activity when pyruvate oxidation is blocked, or when mitochondrial complexes 1 and 2 are inhibited by rotenone and antimycin (R/A) (Fig. 3 *F* and *H*).

Our data show that circulating T cells take up glucose, in sync with their glycolytic metabolic activity used in anaerobic glycolysis. Postactivation, glucose is not acutely critical to supply pyruvate for OXPHOS in circulating $CD8^+$ T cells. IELs more critically rely on glucose uptake upon activation, although this is not critical during a short interval. IELs have a marked capacity for pyruvate oxidation. Importantly, in IELs, OXPHOS is tightly coupled to glycolytic activity, not observed in circulating $CD8^+$ T cells, indicating a close feedback circuit between OXPHOS and glycolysis in IELs.

Activated IELs Have FA Oxidation Capacity. To verify whether the increase in ECAR we observe is indeed correlated with lactate production, we measured lactate in circulating $CD8^+$ T cells and IELs at steady state and 16 h after activation. In line with the obtained ECAR data, we observe an increase in lactate content, intracellular and extracellular, in circulating $CD8^+$ T cells after activation, but this is less marked in IELs (*SI Appendix*, Fig. S3), suggesting that an increase in ECAR in IELs may, in addition, be due to increased CO_2 production as a result of increased OXPHOS activity (Fig. 3*G*). To understand whether IELs depend on other metabolites besides glucose, we assessed T cell requirements for lipid and glutamine oxidation. The inhibition of FAO does not diminish OXPHOS, and no acute capacity for lipids was observed 16 h after circulating $CD8^+$ T cell activation (Fig. 4*A*). As expected, inhibition of FAO does not affect glycolysis in circulating $CD8^+$ T cells (Fig. 4*B*). IELs show no acute dependency on lipid oxidation, but have the capacity for it, and increase OCR and ECAR. In addition, combined inhibition of pyruvate and glutamine availability for oxidation reduced OXPHOS activity, meaning that IEL has a dependency on these metabolites (Fig. 4*C*). Lipid availability for OXPHOS does increase glycolysis. However, reduction in OXPHOS by inhibiting access to pyruvate and glutamate and, subsequently, to lipid availability does inhibit glycolysis in IELs (Fig. 4*D*). Calculated FAO dependency and capacity did not reveal differences between the two activated T cell subsets (Fig. 4 *E* and *F*).

Circulating $CD8^+$ T cells did not show an acute dependency on or capacity for glutamate oxidation (Fig. 4*G*), with none of the inhibitor combinations influencing glycolysis either (Fig. 4*H*). IELs also did not show an acute dependency on or capacity for the oxidation of glutamate (Fig. 4*I*). FAO (Fig. 4 *C* and *D*) and glutamate inhibition (Fig. 4 *I* and *J*) do increase OCR, and, in line with blocking both FAO and glutamate (Fig. 3 *G* and *H*), that sustains energy production and shows maintained or increased ECAR. The latter is possibly explained by the increased OXPHOS and hence more CO_2 production and medium acidification via pyruvate oxidation. Indeed, inhibition with UK-5099 and Etomoxir shows dependency on glucose and lipids as mitochondrial fuel (Fig. 4*I*). This is in line with the capacity of lipids or glucose as mitochondrial fuels (Figs. 3 *G* and *H* and 4 *C* and *D*). In addition, lactate assessment after pyruvate shuttle and FAO inhibition showed that activated circulating $CD8^+$ T cells maintain lactate production. However, blocking mitochondrial access to pyruvate and lipids in activated IELs reveals increased production of lactate (*SI Appendix*, Fig. S3*A*). Combined inhibition of pyruvate and lipid oxidation lowered OXPHOS levels to the minimum, similar to complete mitochondrial complex inhibitors R/A (Fig. 4*I*). Once more, inhibition of OXPHOS in IELs was mirrored by the reduction in glycolysis (Fig. 4*J*). Similarly, the combination of the mitochondria complex inhibitors R/A did not influence glycolysis in circulating T cells, but inhibited glycolysis in IELs (Figs. 3 *C* and *E* and 4 *B*, *D*, *H*, and *J*). Calculated glutamine dependency did not reveal differences between the two activated T cell subsets, but circulating $CD8^+$ T cells do have an increased glutamine capacity (Fig. 4 *K* and *L*).

Our data highlight that, compared with activated circulating T cells, intestinal tissue-resident T cells can use lipids, but especially pyruvate, to enable their OXPHOS capacity. IELs can increase OXPHOS and make optimal use of the product of glycolysis in OXPHOS. Activated IELs produce less lactate; however, this capacity is enhanced when pyruvate oxidation is inhibited.

Glucose Is Determining IEL OXPHOS Activity. IELs have a more rapid OXPHOS burst compared to circulating $CD8^+$ T cells upon in vivo activation yet, at rest, do not reveal this capacity. In addition, IELs depend on glucose for optimal metabolic activity, suggesting that glucose may release IEL activation potential. Acidification rate at steady state is similar between circulating $CD8^+$ T cells and IELs, which alters upon activation (*SI Appendix*, Fig. S4 *A* and *B*). Although glycolysis

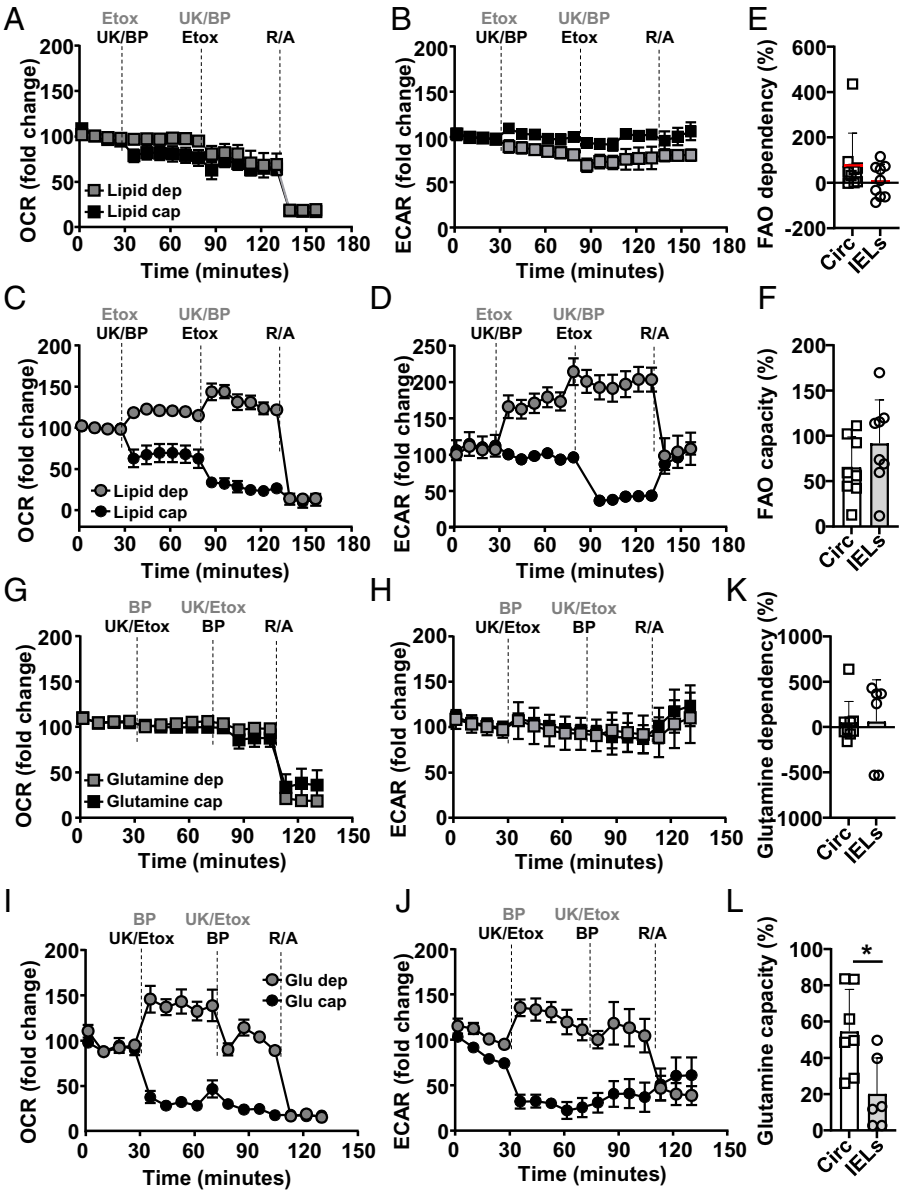

Fig. 4. IELs have capacity but no dependency for lipid oxidation. C57BL/6J mice were injected i.p. with anti-CD3ε, and, at 16 h postactivation, circulating $CD8^+$ T cells (squares) and IELs (circles) were assessed using extracellular flux assessment using the mitofuel assay (compounds indicated at times used) (*A–L*) for dependency or capacity for lipid (*A–F*) or glutamate (*G–L*) oxidation. Normalized (*A* and *C*) OCR and (*B* and *D*) ECAR levels for (*A* and *B*) circulating CD8 T cells or (*C* and *D*) IELs upon addition of Etox to determine lipid dependency (gray symbols, compounds added in gray) or capacity (black symbols and text) after initial inhibition of pyruvate availability with UK (pyruvate carrier [MPC] inhibitor) and glutamate availability with BPTES (BP). (*E* and *F*) Calculated FAO (*E*) dependency or (*F*) capacity (see *Methods*). Normalized (*G* and *I*) OCR and (*H* and *J*) ECAR levels for (*G* and *H*) circulating CD8 T cells or (*I* and *J*) IELs upon addition of BP to determine glutamate dependency (gray symbols, compounds added in gray) or capacity (black symbols and text) after initial inhibition of pyruvate availability with UK (pyruvate carrier [MPC] inhibitor) and lipid availability Etox. (*E* and *F*) Calculated glutamine (*E*) dependency or (*F*) capacity (see *Methods*). Representative of three biological repeats, $n = 2$ to 4. Statistical analysis using Mann–Whitney *U* test; $^*P < 0.05$.

increases in circulating $CD8^+$ T cells upon activation, it is restrained prior to glucose addition (Fig. 5*A*). Within 12 h of activation, glucose supplementation facilitates additional glycolytic activity (Fig. 5 *A* and *B*). Glycolysis reaches maximum levels around 24 h postactivation at near-maximum levels, confirmed by the addition of the ATP synthase inhibitor oligomycin, returning to basal levels by 48 h, the peak of T cell proliferation (Fig. 5*C*). In the absence of exogenous glucose, IEL glycolysis is similarly limited. The addition of glucose increases glycolysis, reaching near-capacity levels swiftly after activation in both T cell subsets (Fig. 5 *A*, *B*, *D*, and *E*). Although IELs can increase their glycolytic activity compared with steady state, the ECAR amplitude compared to circulating $CD8^+$ T cells is lower (Fig. 5 *D–F*). We confirmed that IEL glycolysis is initiated faster compared to circulating T cells, peaking at between 12 and 16 h postactivation, and returning to steady-state levels by 24 h postactivation (Fig. 5 *A–F*). Competitive glucose inhibition via the addition of 2-deoxy-d-glucose (2DG) confirmed the dependency on glucose for glycolysis for both T cell subsets (Fig. 5 *A* and *D*), where the glycolytic reserve is increased in both activated subsets, with higher levels in circulating $CD8^+$ T cells (*SI Appendix*, Fig. S4 *A–C*).

At the same times after activation, we determined OXPHOS levels, observing that basal steady-state levels are similar between IELs and circulating $CD8^+$ T cells (*SI Appendix*, Fig. S4 *D* and *F*). Although pyruvate obtained from glycolysis is used for OXPHOS, OCR levels of circulating $CD8^+$ T cells are not affected over the time period assayed with exogenous

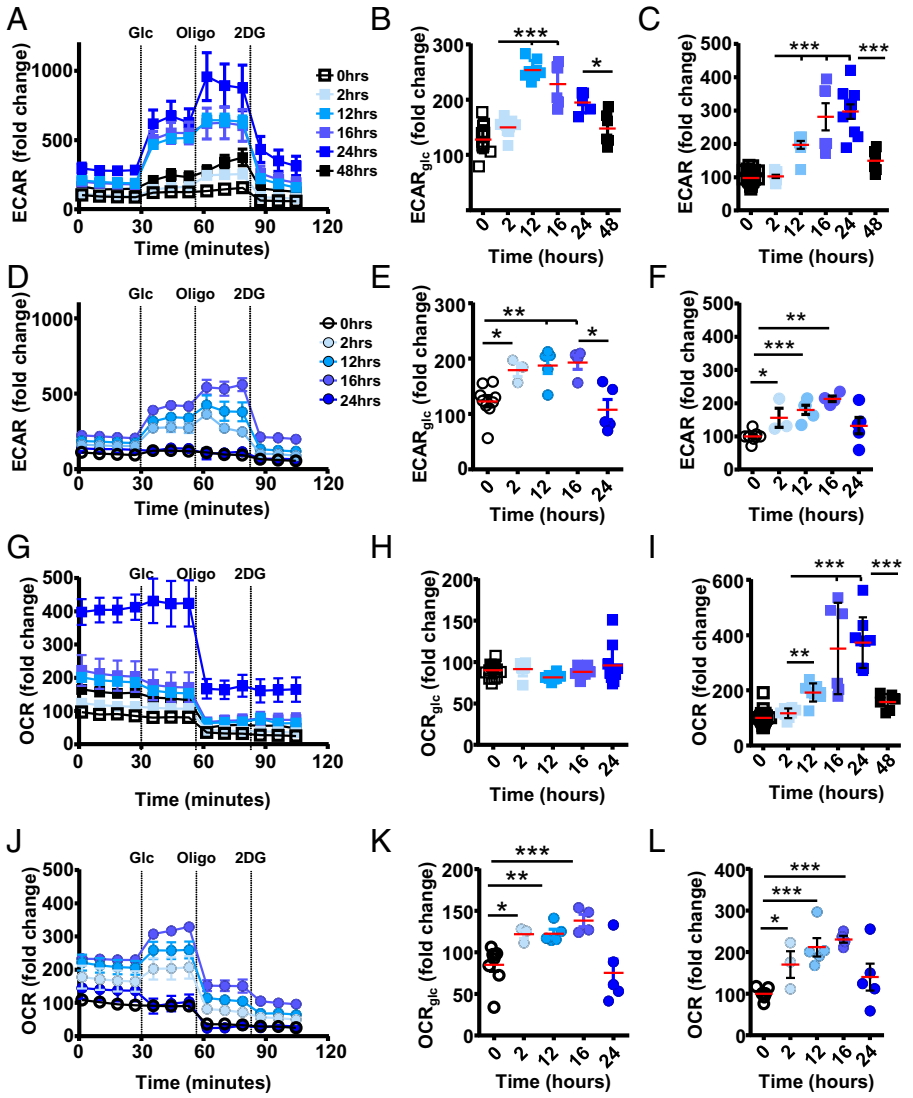

Fig. 5. Activated IELs respond to exogenous glucose with OXPHOS. C57BL/6J mice were injected i.p. with anti-CD3ε, and, from indicated time points, circulating CD8 T cells (squares) and IELs (circles) were assessed for glucose responsiveness using extracellular flux assays. ECAR (*A–F*) and OCR (*G–L*) were assessed for circulating $CD8^+$ T cells (squares) (*A* and *G*) or IELs (circles) (*D* and *J*) using indicated compounds at indicated times (n = 6 to 11, three biological repeats). Data were normalized to the basal level of steady-state conditions (nonstimulated = 100) used at the same time in the same assay. (*B*, *C*, *E*, *F*, *H*, *I*, *K*, and *L*) Plotting fold change upon exogenous glucose addition (glycolytic capacity) compared without (*B*, *E*, *H*, and *K*) and fold change over t = 0 (*C*, *F*, *I*, and *L*). Statistical analysis using Mann–Whitney *U* test; $*P < 0.05$; $**P < 0.01$ $***P < 0.001$.

glucose (Fig. 5 *G* and *H*). This is in agreement with the absence of acute glucose requirements previously observed (Fig. 3*D*). OXPHOS, dependent on mitochondrial activity, is not altered by competitive glucose uptake inhibition. As observed previously, activation of circulating $CD8^+$ T cells results in a robust increase of OXPHOS at 24 h postactivation (Fig. 5 *G* and *I*). In marked contrast, IEL OXPHOS levels show dependency on exogenous glucose (Fig. 5*J*), with OXPHOS activity increasing when glucose is added (Fig. 5 *J* and *K*). This is in agreement with our previously observed acute capacity of IELs for pyruvate (Figs. 3 *G*, *H*, and *J* and 4 *G* and *H*). Similar to glycolysis, the amplitude for OCR in IELs is lower, as observed in circulating T cells (*SI Appendix*, Fig. S4 *E* and *G*). However, OXPHOS levels do increase, similar to glycolysis, peaking at 16 h postactivation, returning to basal levels by 24 h postactivation (Fig. 5*L*). In addition, 2DG, which does not affect OXPHOS activity in circulating $CD8^+$ T cells, reduces OXPHOS in activated IELs, indicating that glucose is an important limiting factor in IEL activation.

Collectively our data show that, although both T cell subsets depend on glucose for their glycolytic activity, circulating $CD8^+$ T cells have no additional capacity to use pyruvate for OXPHOS, while, for IELs glucose, via pyruvate, is a limiting factor for OXPHOS activity. OXPHOS levels in activated circulating T cells are high, without the additional ability to use more glycolysis-derived pyruvate, while OXPHOS in IELs is modest, of shorter duration, and dependent on glycolysis-generated pyruvate.

Metabolite Availability Curtails IEL Function. IELs are ideally positioned to provide a first line of defense against invading pathogens at the epithelial barrier. Few infection models for the small intestine exist. The apicomplexan *Eimeria vermiformis*, a mouse-specific pathogen, infects the epithelia of this organ whereby IEL activity is important for its control, such as observed in the absence of lymphocytes, IL-15 receptor, or the specific reduction in T_{RM} (6, 24). Importantly, glucose feeding of C57BL6/J mice markedly reduced parasite burden, with the

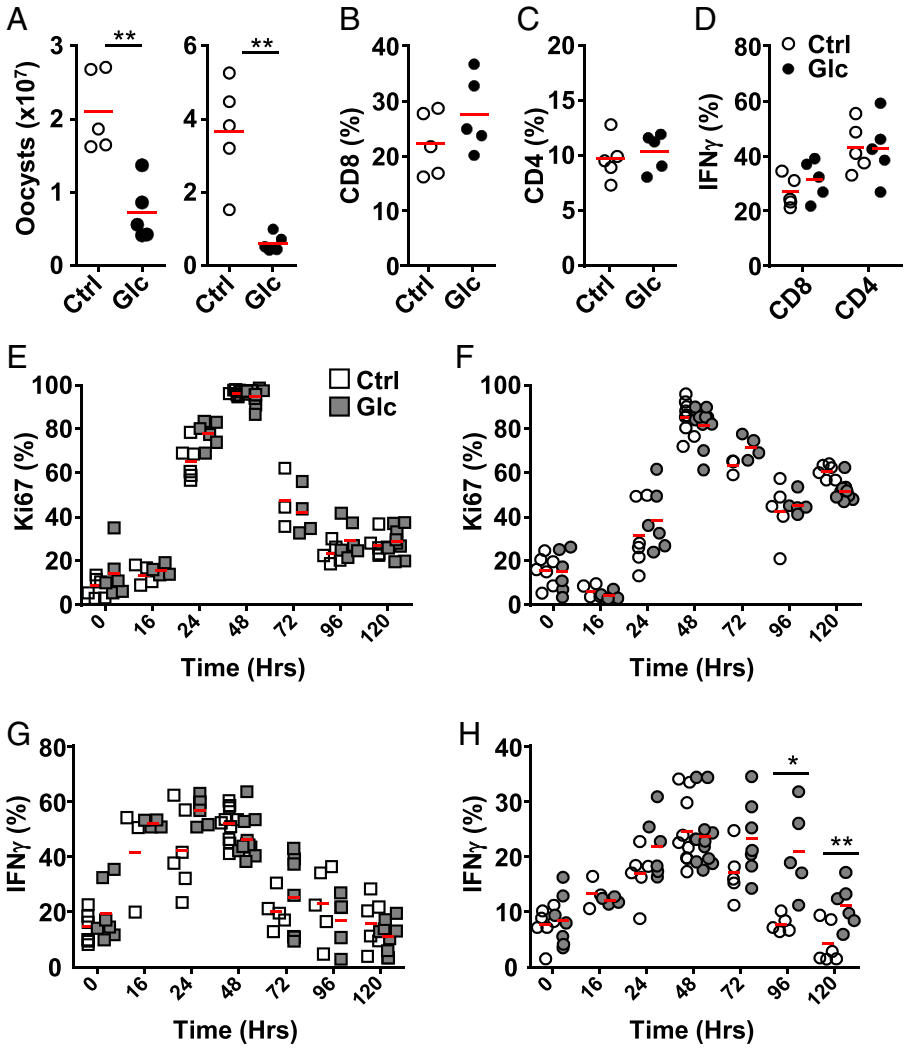

Fig. 6. Acute access to glucose can determine IEL function. C57BL/6J mice were (filled) or were not (open) provided with 10% glucose-containing water. (*A–D*) After 3 d on 10% glucose water, mice were challenged via oral gavage with 1,000 *E. vermiformis* oocysts. (*A*) Oocyst shedding from two biological repeats ($n = 5$), proportion of (*B*) $CD8^+$ and (*C*) $CD4^+$ cells and (*D*) IFNγ production in one representative experiment ($n = 5$). (*E–H*) After 7 d on 10% glucose water, mice were injected i.p. with anti-CD3ε, and circulating $CD8^+$ T cells (squares) or IELs (circles) were assessed for proliferation (*E* and *F*) and IFNγ (*G* and *H*) production (three biological repeats, $n = 2$ to 4). Statistical analysis using Mann–Whitney *U* test; $^*P < 0.05$; $^{**}P < 0.01$.

production of oocysts and in situ parasites reduced at day 10 postinfection compared to controls (Fig. 6*A* and *SI Appendix*, Fig. S5 *A* and *B*). Near the peak of infection, day 10, proliferation of T cells was similar between controls and mice provided with glucose (*SI Appendix*, Fig. S5*C*). At the same time point, proportions of $CD4^+$ and $CD8^+$ T cells are similar between controls and glucose administration in the IEL fraction of the ileum (Fig. 6 *B* and *C*). In addition, we did not observe a difference in the production of IFNγ (Fig. 6*D*).

Due to infections such as *E. vermiformis* initially causing small and local inflammation, it is difficult to detect differences in proliferation or cytokine production early, when IELs are most likely to act, during a heterogeneous immune response in parts of the small intestine. To determine whether dependency on rapid metabolite access has physiological consequences, we activated T cells in vivo with anti-CD3ε antibodies in the presence of additional glucose administered ad libitum in the drinking water. Proliferation of $CD8^+$ T cells circulating or in the IEL compartment was not dependent on glucose (Fig. 6 *E* and *F*). Circulating $CD8^+$ T cells produced IFNγ independent of the additional glucose provided (Fig. 6*G*). Importantly, IELs produced IFNγ for an extended period of time upon glucose feeding, indicating prolonged activity and function (Fig. 6*H*).

Collectively, our results show that IEL activation is controlled by metabolite accessibility, especially glucose. Its availability in the presence of inflammation stimulates IEL activation via glycolysis and interdependent OXPHOS, resulting in full activation and important antimicrobial activity.

Discussion

Epithelial barriers are the portals for microbial invasion. Robust, yet carefully regulated, immune responses are required to avoid dissemination of infectious material or aberrant activation. Tissue-resident $CD8^+$ T cells, such as small-intestinal IELs, are ideally position underneath the single-cell epithelial barrier to respond swiftly, suggested by their arrested activation status, indicating previous activation but without effector molecule production (25). Our data substantiate the semiactivated status of IELs and show their rapid activation potential compared to circulating $CD8^+$ T cells. Importantly, we show that local metabolite availability directly affects IEL function, in marked contrast to circulating $CD8^+$ T cells.

To initiate and optimize function and homing to tissues, migration inhibitors such as CD69 are expressed on T cells that recognize their cognate antigen, to retain them in secondary

lymphoid organs (SLOs) for some time (26). During this time window, available metabolites are taken up, used during T cell proliferation, and stored to enable migration (27). The storage of a variety of metabolites provides flexibility when T cells arrive in the tissues where the microenvironment may be challenging. In line with this, we show that circulating $CD8^+$ T cells obtained from SLOs take up glucose. They show high glycolytic activity that increases within the first 24 h after TCR activation, with a distinct burst in OXPHOS activity around 24 h, and a return to baseline activity within 48 h. The metabolites obtained in the SLOs allow T cell migration and proliferation at sites of infection without acute requirements for exogenous metabolites. In agreement, we show that, upon inhibition of OXPHOS metabolite availability during the time of the extracellular flux assay, circulating T cells maintain high OXPHOS activity. This is maintained even when combinations of inhibitors of the three major metabolic pathways, pyruvate, FA, and glutamate, are used. These inhibitors have no impact on circulating $CD8^+$ T cells over the time of the assay. Only direct inhibition of the mitochondrial respiratory chain complex I and II, with R/A, inhibits OXPHOS in circulating T cells, but not glycolysis, which is maintained. Upon circulating T cell activation, the majority of carbons derived from glucose are not used for anabolic pathways, with much secreted as lactate (28). This does not diminish OXPHOS, which also increases in activated T cells (29). However, despite an increase in glycolysis during activation, we show that OXPHOS is sufficient to sustain metabolic requirements, and it does not have short-term requirements for FAO or glutamate. Furthermore, mitochondrial mass is increased upon activation and in memory $CD8^+$ T cells, increasing OXPHOS capacity (6, 30). In addition, exogenous glucose is able to increase glycolysis, but does not affect OXPHOS. This is in line with reports that mitochondrial activity is maintained, independent of glycolysis, to support circulating $CD8^+$ T cell proliferation (31, 32).

Tissue-resident $CD8^+$ T cells continuously express homing receptors that prevent them from returning to the circulation and tether them to epithelial cells (33). In the small intestine, these characteristically include the expression of CD103 and CD69. A metabolically highly active organ such as the small intestine, geared toward the absorption of metabolites, will have implications for metabolite availability to initiate and sustain immune cells and responses. Despite the absence of SRC at steady state, IEL proliferation kinetics are similar to circulating $CD8^+$ T cells upon in vivo TCR ligation. The steady-state metabolic capacity of IELs resembles the initial activation state of circulating $CD8^+$ T cells, which temporally lose SRC. Others and we have previously shown that metabolism of IELs is altered, with limited capacity for OXPHOS upon mitochondrial uncoupling compared to circulating $CD8^+$ T cells (5, 6, 13). IELs have an altered composition of their mitochondrial membranes, but their composition correlates with their activation status (6). This led us to the hypothesis that stimuli could overcome the apparent block of spare OXPHOS capacity (19). We show that IELs can indeed increase both their glycolytic and OXPHOS capacity, but do this much more rapidly compared with circulating $CD8^+$ T cells. It is interesting to speculate that the absence of SRC of circulating T cells 16 h postactivation may signify the point at which IELs are arrested and, potentially, a point at which circulating $CD8^+$ T cells primarily store energy. This is in line with the peak of OXPHOS in circulating $CD8^+$ T cells around or just after 24 h postactivation, while this peak in IELs can be found around 12 h postactivation.

However, IELs are not simply faster. We show that their activity is regulated by access to metabolites in their immediate environment. IEL rapidly take up and metabolize glucose, using expression of glucose transporters GLUT1, GLUT3, and SGLT1. The latter expressed on high glucose absorptive cells in the small intestine. We used 2-NBDG to understand glucose uptake, but its use in mouse T cells may be limited (21). Therefore, we complemented our assays with 6-NBDG, its uptake competitively inhibited via GLUT1 blocking (20). Exogenous glucose increases glycolysis as in circulating cells, but also increases OXPHOS. This releases IEL metabolic capacity with increased OCR ability. Interestingly, we found that, uniquely in IELs, OXPHOS also affects glycolysis. This occurs when blocking the main tricarboxylic acid cycle metabolic supply routes and by directly inhibiting mitochondrial complexes. Although we confirm that ECAR increase upon activation of circulating $CD8^+$ T cells is correlated with increased lactate production, this is less evident for activated IELs that show an increase in ECAR but limited production of lactate. However, activated IELs increase OXPHOS upon inhibition of FAO or glutamate, which would result in more CO_2 production and decreases the extracellular pH. Collectively, our data suggest that activated IELs require glucose, as shown with high 6-NBDG uptake, and make optimal use of pyruvate for OXPHOS and not the production of lactate. We confirm that activated IELs can produce more lactate when the mitochondrial pyruvate shuttle is blocked, confirming their reliance on glucose. We do not understand the molecular pathway behind the need for glucose, its absence rapidly stopping IEL metabolism. A hypothesis is that IELs have a reduced redox state and insufficient nicotinamide adenine dinucleotide levels to generate the required ATP in the absence of OXPHOS. The coupling of OXPHOS and glycolysis may function as a failsafe, since increased aerobic glycolysis requires glyceraldehyde 3-phosphate dehydrogenase, which, when engaged in glycolysis, does not inhibit IFNγ translation in semiactivated IELs (29). This would ensure that IEL activation is licensed only in the presence of inflammatory and metabolic cues, in line with the extended ability of IFNγ production under high glucose feeding. This also offers therapeutic insights into the regulation of IEL activity, as shown by increasing glucose content in the diet, which increases IEL activity and function. Vice versa, inhibition of glucose metabolism or the important regulator mTOR (target of rapamycin) reduces intestinal immune protection (5).

Inappropriate IEL activity can cause significant immunopathology, damaging the single epithelial layer, causing reduced ability for the host to take up metabolites and liquids, providing pathological and opportunistic microorganisms with circumstances to expand and invade, and may cause significant discomfort to the host (34). Hence, the activity of IELs, which are maintained in a heightened state of activation, contain premade cytolytic enzymes, and contribute to swiftly containing invading microorganism, needs to be tightly controlled. Disruption of barrier physiology and microbiota interactions may contribute to the development of inflammatory bowel disease (IBD), with immune cell activation being an important component (35). Dietary interventions are known to be able to improve IBD disease outcomes, initially thought to act via modulation of the intestinal microbiome, but affecting the intestinal microbiome, as well as epithelial integrity and barrier immune cells (36). However, a metaanalysis study showed that current therapies are less beneficial compared with general immune modulatory steroid therapy (37). General immune suppressive therapies carry risk, and further insights into intestinal tissue immune cell activation requirements, such as their metabolism, will offer the required novel molecular mechanisms and therapeutic potential to counteract IBD. Furthermore, IELs

have recently been show to impact systemic metabolic responses involving diets high in sugar or fat content, thereby influencing general metabolic health (38, 39).

Methods

Mice. C57BL/6J mice were purchased from Charles River. Mice were bred and maintained at the Instituto de Medicina Molecular animal facilities, Lisbon. Mice were systematically compared with cohoused littermate controls unless stated otherwise; 8- to 14-wk-old male and female mice, age and sex matched, were used. All mice were housed in individually ventilated cages (IVC) with temperature-controlled conditions under a 12-h light/dark cycle, and the mice were kept in specific-pathogen-free conditions with free access to drinking water and food. Anti-CD3ε (145-2C11, BioXCell) was given intraperitoneally (i.p.) at 25 μg per animal, 2-NBDG (CAY11046, Cayman Chemical) was given with a retroorbital injection of 100 or 300 μg 1 h before killing. Glucose 10% wt/vol was provided in the drinking water. All animal experimentation complied with the European Union directive and regulations of the Direção-Geral de Alimentação e Veterinária Portugal and local ethical review committee and guidelines.

T Cell Isolation. Spleens were meshed through a 70-μm strainer to obtain a single-cell suspension, and red blood cells were lysed with red blood cells lysis buffer (150 mM NH_4Cl, 10 mM $KHCO_3$, 0.1 mM Na_2EDTA). Small-intestinal IELs were isolated as previously described (12). Briefly, small intestines were flushed with phosphate-buffered saline (PBS) to remove contents, and opened longitudinally. After cutting into 1-cm pieces, samples were incubated in PBS containing 20 mM Hepes, 100 U/mL penicillin, 100 μg/mL streptomycin, 1 mM Pyruvate, 10% fetal calf serum (FCS), 100 μg/mL polymyxin B, and 10 mM EDTA for 30 min at 37 °C while shaking. IEL single-cell suspensions were further enriched using 37.5% isotonic Percoll. Resulting cell fraction was used for fluorescence-activated cell sorter analysis, or CD8α-expressing cells were preenriched by

Table 1. Flow cytometry antibodies used

List of antibodies					
Antigen	Flourochrome	Clone	Supplier	Catalog no.	Validation/technical data sheet
CD8α	APC	53-6.7	BioLegend	100712	https://www.biolegend.com/en-us/products/apc-anti-mouse-cd8a-antibody-150?GroupID=BLG6765
CD8α	SB600	53-6.7	eBioscience	63-0081-82	https://www.thermofisher.com/antibody/product/CD8a-Antibody-clone-53-6-7-Monoclonal/63-0081-82
CD8α	FITC	53-6.7	BioLegend	100706	https://www.biolegend.com/en-us/search-results/fitc-anti-mouse-cd8a-antibody-153?GroupID=BLG2559
CD8α	BV605	53-6.7	BioLegend	100744	https://www.biolegend.com/en-us/products/brilliant-violet-605-anti-mouse-cd8a-antibody-7636?GroupID=BLG2559
CD44	AF700	IM7	BioLegend	103026	https://www.biolegend.com/en-us/products/alexa-fluor-700-anti-mouse-human-cd44-antibody-3406
CD44	PacificB	IM7	BioLegend	103020	https://www.biolegend.com/en-us/products/pacific-blue-anti-mouse-human-cd44-antibody-3099?GroupID=BLG10425
CD8β	PerCP-Cy5.5	YTS156.7.7	BioLegend	126610	https://www.biolegend.com/en-us/search-results/percp-cyanine5-5-anti-mouse-cd8b-antibody-4477
CD8β	AF647	YTS156.7.7	BioLegend	126612	https://www.biolegend.com/en-us/search-results/alexa-fluor-647-anti-mouse-cd8b-antibody-4478?GroupID=BLG4212
CD4	eF506	RM4-5	Invitrogen	69-0042-82	https://www.thermofisher.com/antibody/product/CD4-Antibody-clone-RM4-5-Monoclonal/69-0042-82
CD4	V500	RM4-5	BD Bioscience	560782	https://www.bdbiosciences.com/en-us/products/reagents/flow-cytometry-reagents/research-reagents/single-color-antibodies-ruo/v500-rat-anti-mouse-cd4.560782
TCRβ	PerCP/Cy5.5	H57-597	BioLegend	109228	https://www.biolegend.com/en-us/products/percp-cyanine5-5-anti-mouse-tcr-beta-chain-antibody-5603?GroupID=BLG6996
TCRβ	PacificB	H57-597	BioLegend	109226	https://www.biolegend.com/en-us/products/pacific-blue-anti-mouse-tcr-beta-chain-antibody-4538?GroupID=BLG317
TCRβ	PE	H57-597	BioLegend	109208	https://www.biolegend.com/en-us/products/pe-anti-mouse-tcr-beta-chain-antibody-272?GroupID=BLG6992
CD69	PE-Cy7	H1.2F3	BioLegend	104512	https://www.biolegend.com/en-us/search-results/pe-cyanine7-anti-mouse-cd69-antibody-3168?GroupID=BLG10515
Granzyme B	PacificB	GB11	BioLegend	515408	https://www.biolegend.com/en-us/search-results/pacific-blue-anti-human-mouse-granzyme-b-antibody-8612?GroupID=BLG15670
Ki67	AF647	B56	BD Bioscience	561126	https://www.bdbiosciences.com/en-us/products/reagents/flow-cytometry-reagents/research-reagents/single-color-antibodies-ruo/alexa-fluor-647-mouse-anti-ki-67.561126
IFNγ	FITC	XMG1.2	BioLegend	505806	https://www.biolegend.com/en-us/products/fitc-anti-mouse-ifn-gamma-antibody-995
IFNγ	APC	XMG1.2	BioLegend	505810	https://www.biolegend.com/en-us/products/apc-anti-mouse-ifn-gamma-antibody-993?GroupID=GROUP24

AutoMACS with anti-CD8 beads followed by flow sorting on Aria IIu. Viability and numbers of sorted $CD8^+$ IELs were assessed by live/dead dye (Thermo Fisher, LIVE/DEAD, far red, excitation 633) or DAPI (prior to sell sorting) or trypan blue staining (prior to Seahorse assay).

Flow Cytometry. Single-cell suspensions from spleen and small intestine were prepared and labeled with antibodies (Table 1), according to the agreed standards (40). In brief, IELs or splenic CD8 T cells were resuspended in PBS and stained with fluorescence–conjugated monoclonal antibodies and L10119 LIVE/DEAD Fixable Near-IR staining (cat. L34975, Invitrogen). All fluorochrome-conjugated monoclonal antibodies were purchased from BioLegend. For intracellular cytokine detection, cells were activated for 2 h with 500 ng/mL phorbol 12,13-dibutyrat and 500 ng/mL ionomycin in the presence of 1 μg/mL Brefeldin A (all Sigma) and subsequently stained with anti-TNF or anti-IFNγ fluorescence-conjugated antibodies (BioLegend). Anti-Ki-67 fluorescence-conjugated antibody (BD Biosciences) was used according to the manufacturer's instructions. For 2-NBDG (Cayman Chemical) or 6-NBDG (Carbosynth) uptake in vitro, cells were cultured in PBS containing 50 μg/mL 2-NBDG or 6-NBDG. They were incubated for 50 min at 37 °C with 5% CO_2. Cells were washed in PBS and antibody stained on ice. Analysis using flow cytometry was performed immediately. Samples were run on a Fortessa X-20 cytometer (BD Bioscience) and analyzed with FlowJo X software.

Metabolism Assays.

Mitostress assay. OCR and ECAR were measured in mitostress media (Seahorse DMEM, 25 mM D-glucose, 1 mM L-glutamine, 1% FCS, 1 mM sodium pyruvate, 1% penicillin/streptomycin [P/S]) using a 24-well Extracellular Flux (XF) (Seahorse Bioscience), plating 0.85×10^6 cells per well. OCR and ECAR were measured under basal conditions and after the addition of inhibitors: 1 μM oligomycin, 1.5 μM FCCP, 1 μM rotenone, and 1 μM antimycin with an Extracellular Flux Analyzer.

Glycolysis assay. OCR and ECAR were measured during glycolysis stress test assay in glycolysis media (Seahorse Dulbecco's modified Eagle's medium [DMEM], 1 mM L-glutamine, 1% FCS, 1 mM sodium pyruvate, 1% P/S). Measurements were done under basal condition and after the addition of substances: 10 mM glucose, 1 μM oligomycin, and 20 mM 2DG.

Mitofuel assays. During the mitofuel flex test assay, cells were washed in mitofuel media: DMEM, 10 mM D-glucose, 1 mM sodium pyruvate, 1% P/S, 1 mM glutamine, and 1% FBS. OCR and ECAR were measured under basal conditions. The inhibitors used were 20 μM Etomoxir (FAO inhibitor), 6 μM BPTES (Glutaminase Inhibitor), and 6 μM UK-5099 (Mitochondrial Pyruvate Carrier Inhibitor). Metabolite dependency of circulating T cells and IELs was determined by (baseline OCR – inhibitor OCR)/(baseline OCR – all inhibitors OCR) × 100%. Metabolite capacity of T cell subsets was determined by (1 — (baseline OCR – other two inhibitors OCR)/(baseline OCR – all inhibitors OCR)) × 100%.

Lactate measurements. Circulating $CD8^+$ T cells or $CD8^+$ IELs were flow sorted and cultured in 96-well plates at 1 million cells in 50-μL of Iscove Modified Dulbecco Media (IMDM). After 30 min, 20 μM Etomoxir and 6 μM UK-5099 (Mitochondrial Pyruvate Carrier Inhibitor) or an equal volume of IMDM were added to the wells for 60 min at 37 °C. Subsequently, cells were harvested by centrifugation and washed with PBS, and both medium and cell pellets were stored at −80 °C prior to the assay. Lactate levels were measured enzymatically in 96-well plates according to manufacturer's specifications (Lactate-Glo Assay, Promega, J5022). Briefly, cells were lysed with 0.6N HCl. Cell lysates were neutralized with 1 M Tris-base and incubated in a 1:1 ratio with detection reagent. Extracellular lactate production was measured in the medium with background subtraction from fresh medium. Luminescence was recorded after 1 h, and intracellular and extracellular lactate concentrations were determined from a lactate standard curve. Lactate levels were normalized to cell number.

Histology. Mouse small-intestine tissue samples were fixed in 10% neutral buffered formalin solution (05-K01009, Enzifarma) and histology processed using an overnight protocol in a Tissue HistoCore Pearl (Leica) and embedded in paraffin (ref. #39602012, Leica) in a transversal orientation manner. Three-micrometer-thickness sections were created using a microtome (Minot Microtome Leica RM2145), and stained with hematoxylin (ref. #0506004E. Bio Optica) and eosin (ref. #110132-1L, Sigma) for morphological examination.

Gene Expression Analysis. RNA-sequencing (RNA-seq) libraries were obtained and analyzed as previously described (6), and deposited in the database ArrayExpress, with accession number E-MTAB-6510. Briefly, libraries were constructed using the Tru-Seq sample preparation kit (Illumina), from polyA+ RNAs isolated from purified T cells. RNA-seq was performed on the Hi-Seq 2500 using a 100-base-pair read length program. The barcoded samples were demultiplexed and trimmed with the cutadapt version 1.1 adapter removal software. For the mapping, Ensembl GRCm38 genome annotation together with TopHat alignment software were used. Differential expression analysis was carried out comparing CD8 subsets. All normalizations and differential expression analyses were performed in R (version 3.1.0) together with the DESeq2 Bioconductor package and the Negative Binomial Distribution method.

Infection Challenges. Animals were infected with *E. vermiformis* as previously described in detail (41). Briefly, oocysts were washed three times with deionized water, floated in sodium hypochloride, and counted using a Fuchs–Rosenthal chamber. Mice received 1,000 oocysts of *E. vermiformis* by oral gavage in 100 μL of water and were analyzed at day 10 postinfection. To determine the burden of infection, animals were caged individually, and feces were collected.

Data, Materials, and Software Availability. RNA-seq data have been deposited in the database ArrayExpress, with accession number E-MTAB-6510 (42). All other data are part of the manuscript or *SI Appendix*, and are shown as individual data points in graphs.

ACKNOWLEDGMENTS. We thank the excellent contributions from the Instituto de Medicina Molecular (iMM) flow cytometry, rodent, histology, and microscopy facilities. The project that gave rise to these results has received funding from the following sources:" la Caixa" Foundation under Grant Agreement LCF/PR/HR19/52160005; European Union's Horizon 2020 Research and Innovation Programme under Grant Agreements 667824 and 679168; European Molecular Biology Organization under Grant Agreement IG/3309; Portuguese Foundation for Science and Technology under Grant Agreements IF/01693/2014, UID/BIM/50005/2019, and PTDC/MED-IMU/28003/2017; and European Regional Development Fund through the Lisbon Portugal Regional Operational Program under Grant Agreement PTDC/MED-IMU/28003/2017.

1. A. A. Kolodziejczyk, D. Zheng, E. Elinav, Diet-microbiota interactions and personalized nutrition. *Nat. Rev. Microbiol.* **17**, 742–753 (2019).
2. Š. Konjar, C. Ferreira, B. Blankenhaus, M. Veldhoen, Intestinal barrier interactions with specialized CD8 T cells. *Front. Immunol.* **8**, 1281 (2017).
3. B. Jabri, V. Abadie, IL-15 functions as a danger signal to regulate tissue-resident T cells and tissue destruction. *Nat. Rev. Immunol.* **15**, 771–783 (2015).
4. M. Swamy *et al.*, Intestinal intraepithelial lymphocyte activation promotes innate antiviral resistance. *Nat. Commun.* **6**, 7090 (2015).
5. D. P. Hoytema van Konijnenburg *et al.*, Intestinal epithelial and intraepithelial T cell crosstalk mediates a dynamic response to infection. *Cell* **171**, 783–794.e13 (2017).
6. Š. Konjar *et al.*, Mitochondria maintain controlled activation state of epithelial-resident T lymphocytes. *Sci. Immunol.* **3**, eaan2543 (2018).
7. N. C. Nüssler *et al.*, Enhanced cytolytic activity of intestinal intraepithelial lymphocytes in patients with Crohn's disease. *Langenbecks Arch. Surg.* **385**, 218–224 (2000).
8. M. Kawaguchi-Miyashita *et al.*, An accessory role of TCRgammadelta (+) cells in the exacerbation of inflammatory bowel disease in TCRalpha mutant mice. *Eur. J. Immunol.* **31**, 980–988 (2001).
9. M. D. Buck, R. T. Sowell, S. M. Kaech, E. L. Pearce, Metabolic instruction of immunity. *Cell* **169**, 570–586 (2017).
10. R. Wang *et al.*, The transcription factor Myc controls metabolic reprogramming upon T lymphocyte activation. *Immunity* **35**, 871–882 (2011).
11. A. T. Phan, A. W. Goldrath, C. K. Glass, Metabolic and epigenetic coordination of T cell and macrophage immunity. *Immunity* **46**, 714–729 (2017).
12. Y. Li *et al.*, Exogenous stimuli maintain intraepithelial lymphocytes via aryl hydrocarbon receptor activation. *Cell* **147**, 629–640 (2011).
13. Y. Pan *et al.*, Survival of tissue-resident memory T cells requires exogenous lipid uptake and metabolism. *Nature* **543**, 252–256 (2017).
14. O. J. James, M. Vandereyken, M. Swamy, Isolation, characterization, and culture of intestinal intraepithelial lymphocytes. *Methods Mol. Biol.* **2121**, 141–152 (2020).
15. G. J. van der Windt *et al.*, Mitochondrial respiratory capacity is a critical regulator of CD8+ T cell memory development. *Immunity* **36**, 68–78 (2012).
16. A. M. Fahrer *et al.*, Attributes of gammadelta intraepithelial lymphocytes as suggested by their transcriptional profile. *Proc. Natl. Acad. Sci. U.S.A.* **98**, 10261–10266 (2001).
17. J. Shires, E. Theodoridis, A. C. Hayday, Biological insights into $TCR\gamma\delta^+$ and $TCR\alpha\beta^+$ intraepithelial lymphocytes provided by serial analysis of gene expression (SAGE). *Immunity* **15**, 419–434 (2001).
18. P. M. Gubser *et al.*, Rapid effector function of memory CD8+ T cells requires an immediate-early glycolytic switch. *Nat. Immunol.* **14**, 1064–1072 (2013).

19. M. Veldhoen, B. Blankenhaus, Š. Konjar, C. Ferreira, Metabolic wiring of murine T cell and intraepithelial lymphocyte maintenance and activation. *Eur. J. Immunol.* **48**, 1430–1440 (2018).
20. L. F. Barros *et al.*, Kinetic validation of 6-NBDG as a probe for the glucose transporter GLUT1 in astrocytes. *J. Neurochem.* **109**, 94–100 (2009).
21. L. V. Sinclair, C. Barthelemy, D. A. Cantrell, Single cell glucose uptake assays: A cautionary tale. *Immunometabolism* **2**, e200029 (2020).
22. L. Speizer, R. Haugland, H. Kutchai, Asymmetric transport of a fluorescent glucose analogue by human erythrocytes. *Biochim. Biophys. Acta* **815**, 75–84 (1985).
23. E. H. Ma *et al.*, Metabolic profiling using stable isotope tracing reveals distinct patterns of glucose utilization by physiologically activated $CD8^+$ T cells. *Immunity* **51**, 856–870.e5 (2019).
24. C. Ferreira *et al.*, Type 1 T_{reg} cells promote the generation of $CD8^+$ tissue-resident memory T cells. *Nat. Immunol.* **21**, 766–776 (2020).
25. Š. Konjar, M. Veldhoen, Dynamic metabolic state of tissue resident CD8 T cells. *Front. Immunol.* **10**, 1683 (2019).
26. L. R. Shiow *et al.*, CD69 acts downstream of interferon-α/β to inhibit S1P1 and lymphocyte egress from lymphoid organs. *Nature* **440**, 540–544 (2006).
27. C. J. Fox, P. S. Hammerman, C. B. Thompson, Fuel feeds function: Energy metabolism and the T-cell response. *Nat. Rev. Immunol.* **5**, 844–852 (2005).
28. K. A. Frauwirth *et al.*, The CD28 signaling pathway regulates glucose metabolism. *Immunity* **16**, 769–777 (2002).
29. C. H. Chang *et al.*, Posttranscriptional control of T cell effector function by aerobic glycolysis. *Cell* **153**, 1239–1251 (2013).
30. M. D. Buck *et al.*, Mitochondrial dynamics controls T cell fate through metabolic programming. *Cell* **166**, 63–76 (2016).
31. R. I. Klein Geltink *et al.*, Mitochondrial priming by CD28. *Cell* **171**, 385–397.e11 (2017).
32. E. L. Mills, B. Kelly, L. A. J. O'Neill, Mitochondria are the powerhouses of immunity. *Nat. Immunol.* **18**, 488–498 (2017).
33. L. Barros, C. Ferreira, M. Veldhoen, The fellowship of regulatory and tissue-resident memory cells. *Mucosal Immunol.* **15**, 64–73 (2022).
34. V. Abadie, V. Discepolo, B. Jabri, Intraepithelial lymphocytes in celiac disease immunopathology. *Semin. Immunopathol.* **34**, 551–566 (2012).
35. B. S. Boland *et al.*, Heterogeneity and clonal relationships of adaptive immune cells in ulcerative colitis revealed by single-cell analyses. *Sci. Immunol.* **5**, eabb4432 (2020).
36. A. N. Ananthakrishnan, Epidemiology and risk factors for IBD. *Nat. Rev. Gastroenterol. Hepatol.* **12**, 205–217 (2015).
37. N. Narula *et al.*, Enteral nutritional therapy for induction of remission in Crohn's disease. *Cochrane Database Syst. Rev.* **4**, CD000542 (2018).
38. Z. A. Sullivan *et al.*, γδ T cells regulate the intestinal response to nutrient sensing. *Science* **371**, eaba8310 (2021).
39. S. He *et al.*, Gut intraepithelial T cells calibrate metabolism and accelerate cardiovascular disease. *Nature* **566**, 115–119 (2019).
40. A. Cossarizza *et al.*, Guidelines for the use of flow cytometry and cell sorting in immunological studies (second edition). *Eur. J. Immunol.* **49**, 1457–1973 (2019).
41. P. Figueiredo-Campos, C. Ferreira, B. Blankenhaus, M. Veldhoen, *Eimeria vermiformis* infection model of murine small intestine. *Bio Protoc.* **8**, e3122 (2018).
42. Š. Konjar *et al.*, E-MTAB-6510 - RNA libraries of sorted CD8+ memory T cells from the spleen and RNA libraries of sorted IELs from the small intestine of C57BL/6J mice. ArrayExpress. https://www.ebi.ac.uk/arrayexpress/experiments/E-MTAB-6510. Accessed 10 July 2018.